https://doi.org/10.5194/gmd-2019-256
Preprint. Discussion started: 1 October 2019

Geoscientific Model Development Discussions

The effect of satellite derived leaf area index and roughness length information on modelled reactive nitrogen deposition in north-western Europe.

Shelley C. van der Graaf[1], Richard Kranenburg[2], Arjo J. Segers[2], Martijn Schaap[2,3], Jan Willem Erisman[1,4]

[1]Cluster Earth and Climate, Department of Earth Sciences, Faculty of Science, Vrije Universiteit Amsterdam, Amsterdam, 1081 HV, The Netherlands

[2]TNO, Climate Air and Sustainability, Utrecht, 3584 CB, The Netherlands

[3]Institute for Meteorology, Free University Berlin, Berlin, 12165, Germany

[4]Louis Bolk Institute, Driebergen, 3972, The Netherlands

Correspondence to: Shelley C. van der Graaf (s.c.vander.graaf@vu.nl)

Abstract. The nitrogen cycle has been continuously disrupted by human activity over the past century, resulting in almost a tripling of the total reactive nitrogen fixation in Europe. Consequently, excessive amounts of reactive nitrogen (N_r) have manifested in the environment, leading to a cascade of adverse effects, such as acidification and eutrophication of terrestrial and aquatic ecosystems, and particulate matter formation. Chemistry transport models (CTM) are frequently used as tools to simulate the complex chain of processes that determine atmospheric N_r flows. In these models, the parameterization of the atmosphere-biosphere exchange of N_r is largely based on few surface exchange measurement and is therefore known to be highly uncertain. In addition to this, the input parameters that are used here are often fixed values, only linked to specific land use classes. In an attempt to improve this, a combination of multiple satellite products is used to derive updated, time-variant leaf area index (LAI) and roughness length (z_0) input maps. As LAI, we use the MODIS MCD15A2H product. The monthly z_0 input maps presented in this paper are a function of satellite-derived NDVI values (MYD13A3 product) for short vegetation types (such as grass and arable land) and a combination of satellite-derived forest canopy height and LAI for forests. The use of these growth-dependent satellite products allows us to represent the growing season more realistically. For urban areas, the z_0 values are updated, too, and linked to a population density map. The approach to derive these dynamic z_0 estimates can be linked to any land use map and is as such transferable to other models. We evaluated the resulting changes in modelled deposition of N_r components using the LOTOS-EUROS CTM, focusing on Germany, the Netherlands and Belgium. The implementation of these updated LAI and z_0 input maps led to local changes in the total N_r deposition of up to ~30% and a general shift from wet to dry deposition. The most distinct changes are observed in land use specific deposition fluxes. These fluxes may show relatively large deviations, locally affecting estimated critical load exceedances for specific natural ecosystems.

https://doi.org/10.5194/gmd-2019-256
Preprint. Discussion started: 1 October 2019

Geoscientific Model Development Discussions

1. Introduction

The nitrogen (N) cycle has been continuously disrupted by human activity over the past century (Fowler et al., 2015;Galloway et al., 2004;Galloway et al., 2008), resulting in a doubling of the total reactive nitrogen (N_r) fixation globally and even a tripling in Europe. As a result, excessive amounts of N_r, defined as all N compounds except N_2, have manifested in the environment contributing to acidification and eutrophication of sensitive terrestrial and aquatic ecosystems (Bobbink et al., 2010a;Paerl et al., 2014). NO_x and NH_3 affect air quality through their significant role in the formation of particulate matter, impacting human health and life expectancy (Lelieveld et al., 2015;Bauer et al., 2016;Erisman and Schaap, 2004). N_r also influences climate change through its impact on greenhouse gas emissions and radiative forcing (Erisman et al., 2011;Butterbach-Bahl et al., 2011). As N_r forms are linked through chemical and biological conversion in one another within the environmental compartments, one atom of N may even take part in a cascade of N_r forms and effects (Galloway et al., 2003). To minimize these adverse effects, effective nitrogen management and policy development, therefore, require consideration of all N_r forms simultaneously.

With the scarceness and inadequate distribution of available ground measurements, especially for reduced N_r, the most important method to assess and quantify total N_r budgets on a larger spatial scale to date remains the use of models. Models, chemistry transport models, in particular, are used for understanding the atmospheric transport and the atmosphere-biosphere exchange of nitrogen compounds. Most chemistry transport models compare reasonably with observations for oxidized forms of N_r, but need improvement when it comes to the reduced forms of N_r (Colette et al., 2017). Modelled NH_3 fields are in general uncertain due to the highly reactive nature and the uncertain lifetime of NH_3 in the atmosphere. More importantly, NH_3 emissions that are used as model input are very complex to estimate and remain highly uncertain (Reis et al., 2009;Behera et al., 2013), for example, due to the diversity in NH_3 volatilization rates originating from different agricultural practices. Recently, a lot of effort has been made to improve the spatiotemporal distributions of bottom-up NH_3 emissions (e.g. (Hendriks et al., 2016;Skjøth et al., 2011). Emissions can also be estimated top-down through the usage of data assimilation and inversion techniques. Optimally combining observations and chemistry transport models have already enabled us to create large-scale emission estimates for various pollutants (e.g. (Curier et al., 2014;Abida et al., 2017), for instance for NO_2, and will likely also be used for large-scale NH_3 emission estimates in the future.

Most data assimilation and inversion methods rely on the assumption that sink terms in the model hold a negligible uncertainty. To obtain reasonable top-down emission estimates, we must thus also aim to reduce the uncertainty involved on this side of models. The sink strengths of trace gases and particles in chemistry transport models are often pragmatic and computed with relatively simple empirical functions (e.g. following (Wesely, 1989;Emberson et al., 2000;Erisman et al., 1994)), mostly linked to land use classification maps. The parameterization of the atmosphere-biosphere exchange of N_r components that is used in models is largely based on surface exchange measurements and is therefore very uncertain, especially for NH_3 (Schrader et al., 2016). The deposition strengths in models may vary tremendously depending on the used deposition parameterisation and velocities (Wu et al., 2018;Schrader and Brummer, 2014). Moreover, inter-model discrepancies in deposition fluxes may also arise from

https://doi.org/10.5194/gmd-2019-256
Preprint. Discussion started: 1 October 2019

Geoscientific Model Development Discussions

differences in the used input variables. Here, we focus on the leaf area index (LAI) and the roughness length (z_0) input values. The deposition velocity is often parameterized using both the LAI and the z_0. Currently, most models use fixed, land use specific values for both parameters. In practice, however, spatial as well as seasonal variation is observed. In this paper, we aim to improve the deposition flux modelling by using more realistic, spatial- and time-variant LAI and z_0 values that are derived from optical remote sensors.

The LAI is defined as the one-sided green leaf area per unit surface area (Watson, 1947). The LAI serves as a measure for the amount of plant canopy, and herewith directly related to energy and mass exchange processes. As a result, the LAI is nowadays used as one of the main parameters in many ecological models. In deposition modelling, stomatal uptake is often parameterised using the LAI. The LAI can be determined in the field using either direct methods, such as leaf traps, or indirect methods, such as hemispherical photography (Jonckheere et al., 2004). Another group of indirect methods to estimate the LAI is the use of optical remote sensing. The LAI can, for instance, be estimated using empirical relationships between LAI and vegetation indices (e.g. (Soudani et al., 2006;Davi et al., 2006;Turner et al., 1999) or by inversion of canopy reflectance models (e.g. (Houborg and Boegh, 2008;Myneni et al., 2015). A well-known example of the latter is the LAI product from the MODIS instrument, which we will use in this study.

The z_0 is used to describe the surface roughness. The surface roughness serves as a momentum sink for atmospheric flow and is, therefore, an important term in atmospheric modelling. The interaction between the boundary layer and the roughness of the Earth's surface results in shear stress that affects the wind speed profile. Under neutral conditions, the resulting logarithmic wind profile is defined as:

$$U(z) = \frac{u_*}{k} ln\left(\frac{z}{z_0}\right) \quad \text{(eq. 1)}$$

$U(z)$ represents the mean wind speed, u_* the friction velocity and k the Von Kármán constant. Here, z_0 is a constant that represents the height at which the wind speed theoretically becomes zero. The z_0 can be estimated from in-situ wind speed measurements using bulk transfer equations. More recently, several studies have shown that z_0 for specific, uniform land cover types can also be estimated from optical remote sensing measurements, for instance using vegetation indices (e.g. (Xing et al., 2017;Yu et al., 2016;Bolle and Streckenbach, 1993;Hatfield, 1988;Moran, 1990)). The z_0 can also be estimated using (satellite-derived) vegetation height (e.g. (Raupach, 1994;Plate, 1971;Brutsaert, 2013;Schaudt and Dickinson, 2000)).

The use of optical remote sensing data holds promising potential for improvements of the representativeness of the surface characterization in chemistry transport models. Here, we illustrate the effect of replacing the default implementation with new, satellite-based LAI and z_0 maps on transport and deposition modelling of N_r components. We evaluate the changes in N_r deposition and distribution fields, focusing on Germany, the Netherlands and Belgium. Moreover, we quantify and present the implications for land use specific fluxes on a model subpixel level. Also, we compare our model outputs with wet deposition measurements of NH_4^+ and NO_3^- and surface concentration measurements of NH_3 and NO_2.

https://doi.org/10.5194/gmd-2019-256
Preprint. Discussion started: 1 October 2019

Geoscientific Model Development Discussions

2. Model and datasets

2.1. LOTOS-EUROS

2.1.1. Model description

The LOTOS-EUROS model is a Eulerian chemistry transport model that simulates air pollution in the lower troposphere (Manders et al., 2017). In this study the horizontal resolution is set to 0.125º by 0.0625º, corresponding to pixels of approximately 7 by 7 kilometres in size. The model uses a five-layer vertical grid that extends up 5 km above sea level, starting with a surface layer with a fixed height of 25 meters. The next layer is a mixing layer, followed by two time-varying dynamic reservoir layers of equal thickness, and a top layer up to 5 km. LOTOS-EUROS follows the mixed layer approach and performs hourly results using ECMWF meteorology (European Centre for Medium-Range Weather Forecasts, 2016). The gas-phase chemistry uses the TNO CBM-IV scheme (Schaap et al., 2009) and the anthropogenic emissions from the TNO-MACC-III emission database (Kuenen et al., 2014). LOTOS-EUROS makes use of the CORINE/Smiatek land use map to determine input values for surface variables.

2.1.2. Dry deposition module

The dry deposition flux of gases is computed following the resistance approach, in which the exchange velocity V_d is equal to the reciprocal sum of the aerodynamic resistance R_a, the quasi-laminar boundary layer resistance R_b and the canopy resistance R_c:

$$V_d = \frac{1}{R_a + R_b + R_c} \quad \text{(eq. 1)}$$

$R_a(z_0, \dots)$ is computed using stability parameters and the function proposed by Businger et al. (1971). $R_b(z_0, \dots)$ follows the parameterization presented in McNaughton and Van Den Hurk (1995). R_a and R_b are both influenced by the wind profile. The wind profile, in turn, depends on the z_0 associated with different land use classes. An extensive description of the calculation of R_a and R_b can be found in Manders-Groot et al. (2016). The canopy resistance $R_c(\mathrm{LAI}, \dots)$ is computed using the DEPAC3.11 (Deposition of Acidifying Compounds) module (van Zanten et al., 2010). R_c is a parallel system of the resistances of three different pathways, the external leaf surface or cuticular resistance R_w, the effective soil resistance $R_{soil,eff}$ and the stomatal resistance R_s, and is defined as:

$$R_c = \left(\frac{1}{R_w} + \frac{1}{R_{soil,eff}} + \frac{1}{R_s} \right)^{-1} \quad \text{(eq. 2)}$$

The parameterizations of R_w, $R_{soil,eff}$ and R_s differ with land use types. The LAI, therefore, has a varying influence on the computation of R_c for each land use type. The CORINE/Smiatek land use categories are assigned to the nine different land use classes that are used in DEPAC. LOTOS-EUROS uses a fixed z_0 value for each of these land use classes. The default LAI values are also linked to the DEPAC classes, and follow a fixed temporal behaviour that describes the growing season of each land use class (Emberson et al., 2000). The bi-directional exchange of NH_3 is

https://doi.org/10.5194/gmd-2019-256
Preprint. Discussion started: 1 October 2019

included in the implementation of the DEPAC3.11 module (Wichink Kruit et al., 2012), allowing emissions of NH_3 under certain atmospheric conditions. More information about the most recent version of the model can be found in Manders et al. (2017).

2.2. Datasets

The following section gives a short description of all the datasets that are used in this study. Firstly, a description of the LAI dataset is given. Subsequently, the datasets that are used to derive the updated z_0 maps are described. Finally, the in-situ observations that are used for the validation of the modelled N_r deposition and concentration fields are discussed in the last paragraph.

2.2.1. MCD15A2H Leaf Area Index

The satellite-derived Leaf Area Index (LAI) is a combined product of the MODIS instruments on board the Terra and Aqua satellites (Myneni et al., 2015). The LAI algorithm compares bidirectional spectral reflectances observed by MODIS to values evaluated with a vegetation canopy radiative transfer model that are stored in a look-up table. The algorithm then archives the mean and the standard deviation of the derived LAI distribution functions. We used the 6th version of the product, MCD15A2H, which has a temporal resolution of 8 days and a spatial resolution of 500 meters.

2.2.2. MYD13A3 NDVI

The Normalized Difference Vegetation Index (NDVI) is a vegetation index computed with reflectances observed by the MODIS instrument on board of the Aqua satellite (Didan, 2015). The NDVI is the normalized transform of the near infrared to the red reflectance and is expressed by:

$$\mathrm{NDVI} = \frac{\rho_{\mathrm{NIR}} - \rho_{\mathrm{red}}}{\rho_{\mathrm{NIR}} + \rho_{\mathrm{red}}} \qquad \text{(eq. 3)}$$

We used the MYD13A3 product, which is the monthly NDVI product with a spatial resolution of 1 km.

2.2.3. Forest canopy height

The forest canopy height is derived from LIDAR (Light Detection And Ranging) data acquired by the GLAS (Geoscience Laser Altimeter System) instrument aboard the ICESat (Ice, Cloud, and land Elevation Satellite) satellite (Zwally et al., 2002). This instrument was an altimeter that transmitted a light pulse of 1024 nm and recorded the reflected waveform. We used the global forest canopy height product developed by Simard et al. (2011), which has a spatial resolution of 1 km.

2.2.4. Population density map

The population density grid used in this study available for all European countries and provided by the European Environmental Agency (Gallego, 2010). The population density is disaggregated with the CORINE Land Cover

https://doi.org/10.5194/gmd-2019-256
Preprint. Discussion started: 1 October 2019

Geoscientific Model Development Discussions

inventory of 2000, using data on population per commune. The resulting population density grid is downscaled to a spatial resolution of 100 meters.

2.2.5. CORINE Land Cover

The CORINE Land Cover (CLC) is a land use inventory that consists of 44 classes (European Environmental Agency, 2014). The CLC is produced by computer-assisted visual interpretation of a collection of high resolution satellite images. The CLC has a minimum mapping unit of 25 ha and a thematic accuracy of >85%. We used the latest version of the product, CLC 2012, in this study.

2.2.6. In-situ observations

The modelled NH_4^+ and NO_3^- wet deposition fluxes are compared to observations of wet-only samplers. We used observation from the Dutch LMRe network (Van Zanten et al., 2017) and the German Lander network (Schaap et al., 2017).The location of the stations can be found in Figure 12. The modelled NH_3 surface concentrations are compared to observation from the Dutch MAN network (Lolkema et al., 2015) and the European EMEP network (EMEP, 2016). The modelled NO_2 surface concentrations are compared to observation from AirBase (EEA, 2019). We only used background stations. The location of these stations can be found in Figure 18.

3. Methodology

3.1. Updated z_0 maps

The updated z_0 maps are a composition of z_0 values derived using different methods. We distinguish three different main approaches: 1) z_0 values that depend on forest canopy height, 2) z_0 values that depend on the NDVI and 3) new z_0 values for urban areas that depend on the population density map. In addition to these three approaches, the z_0 values of some urban classes were set to new default values. An overview of the datasets that are used for each DEPAC land use class is given in Table 1.

The MODIS NDVI, the MODIS LAI and the GLAS forest canopy height had to be pre-processed and homogenized in order to obtain consistent input maps that can be read into the LOTOS-EUROS model. To achieve this, we created input maps for each DEPAC class on the coordinate grid of the CORINE/Smiatek land use map in LOTOS-EUROS.

First of all, the original datasets were re-projected to geographic coordinates. To deal with the different horizontal resolution of these datasets the CLC2012 map, having the highest horizontal resolution, was used as a basis for the computation of the updated z_0 values. The first step was to isolate homogeneous pixels within each dataset, which we defined as pixels that consist of over 85% of one individual CORINE land cover class. For each pixel of the datasets, we computed the percentages of each CORINE land cover class within that pixel. The pixels with percentages higher than 85% were isolated for each CORINE land cover class. We used the remaining pixels to compute z_0 values for each CORINE land cover class. The methods that were applied are described in the subsequent section.

https://doi.org/10.5194/gmd-2019-256
Preprint. Discussion started: 1 October 2019

Geoscientific Model Development Discussions

3.1.1. Forest canopy height derived z_0 values

The forest canopy height dataset derived from GLAS LiDAR observations is used to compute the z_0 values for each CLC2012 forest land cover class (broad-leaved forest, coniferous forest and mixed forest) that corresponds to one of the DEPAC forest land use classes (4: coniferous forest and 5: deciduous forest). Several publications relate vegetation height to z_0 (e.g. (Raupach, 1994;Plate, 1971;Brutsaert, 2013)). Here we used the often used equation from (Brutsaert, 2013):

$$z_0 = 0.136 * h \quad \text{(eq. 4)}$$

The vegetation height is the most important parameter influencing turbulence near the surface, and for this reason the used parameterisation gives a reasonable estimate of z_0, even though it ignores many other aspects that influence z_0 (e.g. density, vertical distribution of foliage). Multiple studies have illustrated that there is a seasonal variation in z_0/h for different types of forests (e.g. (Yang and Friedl, 2003;Nakai, 2008)). The z_0 of deciduous trees is therefore additionally linked to the leaf area index to account for changes in tree foliage. The following formula is used to compute the monthly z_0 value for each deciduous forest pixel:

$$z_0(LAI) = z_{0,min} + \frac{LAI - LAI,min}{LAI,max - LAI,min}(z_{0,max} - z_{0,min}) \quad \text{(eq. 5)}$$

Here the maximum roughness length $z_{0,max}$ is set to the LiDAR-derived z_0 from (eq. 4). The minimum roughness length $z_{0,min}$ represents the z_0 of leafless deciduous trees. Following the dependence of z_0/h on LAI presented in Nakai (2008) and Yang and Friedl (2003), we set the $z_{0,min}$ to 80% of $z_{0,max}$.

3.1.2. NDVI derived z_0 values

Table 1 gives an overview of several studies that relate the z_0 value to the NDVI. The functions are derived for different vegetation types under specific conditions. Equations 6 to 12 are derived for different types of agricultural land. The equations are all within a reasonable range from one another for NDVI values lower than ~0.8. Therefore, we chose to use the average function of eq. 6 to eq. 11 to compute z_0 values for all CLC subcategories of the following DEPAC classes: “arable”, “other” and “permanent crops”. Figure 2 is a visualization of eq. 6 to 11 and the used mean function. The z_0 value of grasslands is in general lower than other vegetation types. The last equation, eq. 12, is specifically derived for grassland and is therefore used for all CLC subcategories that fall under the DEPAC class “grass”.

3.1.3. z_0 values for urban areas

The default z_0 of urban areas in LOTOS-EUROS was set to 2 meters. We have updated the z_0 values for urban areas to avoid possible overestimation of z_0 in sparsely populated urban areas. The updated z_0 values for CLC2012 class 1 and 2, ‘1: continuous urban fabric’ and ‘2: discontinuous urban fabric’ are time-invariant and coupled to the EEA population density map. The z_0 values are set to 2 metres in areas with a population density higher than 5000

https://doi.org/10.5194/gmd-2019-256
Preprint. Discussion started: 1 October 2019

Geoscientific Model Development Discussions

inhabitants/km^2 and to 1 metre in areas with a population density lower than 5000 inhabitants/km^2. The z_0 values of the other urban subcategories, CLC2012 class 3 to 9, are updated to the proposed values for CLC classes in (Silva et al., 2007).

3.2. LAI and z_0 in LOTOS-EUROS

After the computation of the z_0 values, the maps for each CORINE land cover class were merged and converted into DEPAC classes using a pre-defined conversion table. As multiple CORINE land cover may translate to one single DEPAC class, the weighted average based on the respective percentage of each CORINE land cover class was computed for each pixel. We then used linear interpolation to obtain continuous z_0 maps for each DEPAC class. Finally, the maps were re-gridded unto the CORINE/Smiatek grid and saved into one file per month.

The default parameterization of the LAI in LOTOS-EUROS is replaced by the MCD15A2H LAI product from MODIS. First, we applied a coordinate transformation to obtain the data in geographical coordinates. The data was then re-gridded unto the grid of the CORINE/Smiatek land use map using linear interpolation. The quality tags were evaluated to identify pixels with default fill values from the MCD15A2H product. These fill-values were replaced by the default LAI values in LOTOS-EUROS, to avoid modelling discrepancies resulting from sudden jumps in LAI values. Finally, the values were sorted per DEPAC land use class and individual fields were created for each class as new input for LOTOS-EUROS.

4. Results

4.1. Comparison of the default and updated z_0 values

We used the CORINE/Smiatek land use map to combine all the updated z_0 values into one single map. The resulting composite map has a horizontal resolution of 500 by 500 metres and is shown in Figure 2.

The mean relative difference (MRD) between the default and updated z_0 values is presented in Figure 3. The largest positive differences occur in forested areas, meaning that the default z_0 values are lower than the updated z_0 values. The largest negative deviations occur in urban areas and areas with “grass”. The updated z_0 values are generally lower in the Netherlands and Belgium, and mostly higher in Germany.

Figure 4 shows the seasonal variation of the updated z_0 values for each of the time-variant DEPAC classes. The black line represents the monthly mean z_0 and the ranges the standard deviation of the z_0 values. Table 3 gives an overview of the default z_0 values in LOTOS-EUROS and the mean and standard deviation of the new z_0 values for each of the DEPAC land use classes. The updated z_0 values for “arable land”, “coniferous forest”, “deciduous forest” and “other” are on average higher than the default z_0 values in LOTOS-EUROS. The updated z_0 values for “grass”, “permanent crops” and “urban” are on average lower than the default z_0 values in LOTOS-EUROS.

https://doi.org/10.5194/gmd-2019-256
Preprint. Discussion started: 1 October 2019

Geoscientific Model Development Discussions

4.2. Comparison of the default and MODIS LAI

The yearly mean MODIS LAI values are shown in Figure 5. The mean differences between the MODIS and the default LAI values are presented in Figure 6. The largest positive differences occur in areas with "arable land", where the mean default LAI values are lower than the MODIS LAI values. The largest negative deviations occur in areas with forest, especially for "coniferous forest". The yearly variation of the MODIS and the default LAI values are shown in Figure 7. The default LAI of "grass" and "deciduous forest" seems to fit the yearly variation of the MODIS LAI quite well.

4.3. Implications for modelled N_r deposition fields

In the following section, the impact of the updated LAI and z_0 values on modelled N_r deposition fields in LOTOS-EUROS is discussed. A total of four different LOTOS-EUROS runs are compared to examine the individual effect of the updated LAI and z_0 values on the modelled N_r distributions and deposition fields. The first run, named "$LE_{default}$", is the standard run using default LAI and z_0 values. The second run, named "LE_{LAI}", uses updated LAI values and the default z_0 values. The third run, named "LE_{z0}", uses updated z_0 values and the default LAI values. The fourth run, named "LE_{z0+LAI}", uses both updated LAI and z_0 values. From now on, we will refer to the outputs of these different runs using the abovementioned abbreviations.

4.3.1. Effect on total N_r deposition

Figure 8 shows the division of the total terrestrial N_r deposition over Germany, the Netherlands and Belgium into different N_r compounds for each of the model runs. A relatively larger portion of the total N_r deposition is attributed to oxidized forms of N_r in Germany. The reduced forms of N_r predominate in the Netherlands and Belgium. The largest change in total N_r deposition occurs in Belgium (+6.19%) due to the inclusion of the MODIS LAI. This corresponds to the relative increase in LAI values here. The inclusion of the updated z_0 values lead to a minor decrease in total N_r deposition in the Netherlands (-1.45%) and Belgium (-1.13%), and a minor increase in Germany (+0.44%).

4.3.2. Effect on wet and dry N_r deposition

We examined the direct effect of the updated LAI and z_0 values on the modelled dry N_r deposition, as well as the related indirect effect in modelled wet N_r deposition. Figure 9 shows the dry and wet N_r deposition in kg N ha^{-1} in 2014, modelled with the updated LAI and z_0 values as input in LOTOS-EUROS. Figure 10 shows the relative changes in the total amount of dry and wet N_r deposition of the different runs with respect to the default run. The combined effect shows an increase of the amount of dry N_r deposition over most parts of Belgium and Germany. The amount of wet N_r deposition decreases over most parts of Germany and eastern Belgium, but remains unchanged in north-western parts of Germany. We observe a decrease in total N_r deposition in the Netherlands. In general, we observe changes ranging from approximately -20% to +30% in the total amount of dry N_r deposition. The changes in wet N_r deposition are smaller in magnitude, and range from approximately -3% to +3%.

https://doi.org/10.5194/gmd-2019-256
Preprint. Discussion started: 1 October 2019

Geoscientific Model Development Discussions

4.3.3. Effect on reduced and oxidized N_r deposition

We split up the total Nr deposition into NH_x (NH_3 and NH_4^+) and NO_y (NO and NO_2 and NO_3^- and HNO_3) deposition, to look at the effect of the updated LAI and z_0 input maps on the deposition of reduced and oxidised forms of N_r, respectively. Figure 11 shows the modelled NH_x and NO_y deposition in kg N ha^{-1} in 2014, including the updated LAI and z_0 input values. Figure 12 shows the relative changes (%) in the total NH_x and NO_y of the different runs with respect to the default run of LOTOS-EUROS. The updated z_0 values have a larger impact on the NH_x deposition than on the NO_y deposition. The implementation of the updated z_0 values has led to a decrease in NH_x deposition over most of the Netherlands, and western Belgium, driven by the large fraction of grassland here. The updated LAI values led to relatively more NH_x deposition in Belgium. The updated LAI values led to an increase of NO_y deposition in almost all areas within the modelled region, except for some urban areas. Moreover, the impact seems to be limited in large forests located in background areas.

4.3.4. Effect on land use specific fluxes

Table 4 gives an overview of changes in the distribution of the land use specific fluxes in the whole study area (Germany, the Netherlands and Belgium combined) for the different runs. The most distinct changes in N_r deposition are due to the updated LAI values ("LE_{LAI}"), where we observe an increase in total N_r deposition on urban areas (+ 16.62%) and arable land (+ 9.53%), and a decrease on coniferous forests (- 9.36%). This coincides with the categories where we observe the largest changes in LAI values. The default LAI values in urban areas were first set to zero for all urban DEPAC categories. The MODIS LAI values, however, are only zero in densely populated areas and areas with industry. The main effects of the updated z_0 values ("LE_{z0}") can be observed for grass (-3.95 %), permanent crops (+ 3.27) and arable land (-3.17 %). In the combined run, "LE_{z0+LAI}", we observe an amplified effect in total N_r deposition over grass (- 8.05%) and arable land (+ 12.88%). The impact of the individual parameters on the remaining land use categories are attenuated in this run.

4.4. Implications for N_r distributions

The changes in N_r deposition amounts induce an effect in the modelled distribution of nitrogen components. Here, we look at the effect of the updated LAI and z_0 values on NH_3 and NO_2 surface concentrations. Figure 13 shows the updated modelled NH_3 and NO_2 surface concentrations in 2014. The dots on top of the figures represent the stations that are used for validation, and their observed mean NH_3 and NO_2 surface concentrations. Figure 14 shows the relative change in yearly mean NH_3 and NO_2 surface concentrations in 2014 of the different runs with respect to the default run of LOTOS-EUROS.

The first column represents the changes in NH_3 and NO_2 surface concentrations due to the updated z_0 values. The NH_3 surface concentration in the Netherlands has increased by up to ~8%. The NH_3 surface concentration in almost all of Germany has decreased by up to ~10%. The changes in the NO_2 surface concentration are less distinct and changed approximately minus to plus 4% in most areas. The middle column represents the changes in NH_3 and NO_2 surface concentrations due to the inclusion of the MODIS LAI only. The NH_3 surface concentration has increased

https://doi.org/10.5194/gmd-2019-256
Preprint. Discussion started: 1 October 2019

Geoscientific Model Development Discussions

with up to ~10% in the Netherlands, western Belgium and north-western and southern Germany. The NH_3 surface concentration has decreased in eastern Belgium and central Germany. The NO_2 surface concentrations have decreased with up to ~6% in almost all of the modelled area.

4.5. Comparison to in-situ measurements

To analyse the effect of the updated LAI and z_0 values, we compared our model output to the available in-situ observations. Due to the lack of available dry deposition measurements, we decided to use NH_4^+ and NO_3^- wet deposition and NH_3 and NO_2 surface concentrations measurements instead. The distribution of the wet deposition stations is shown in Figure 15, as well as the modelled mean NH_4^+ (left) and NO_3^- (right) wet deposition in 2014. The locations of the stations that measure the NH_3 and NO_2 surface concentrations are shown in Figure 13.

The relationships between the modelled and observed fields are evaluated using the Pearson's correlation coefficient (r), the root-mean-square error (RMSE) and the coefficients (slope, intercept) of simple linear regression. Table 6 shows these measures for the comparison with monthly mean NO_3^- wet deposition, NH_4^+ wet deposition, and the monthly mean NH_3 and NO_2 surface concentrations in 2014. Overall, we do not observe large changes in the shown measures due to the inclusion of the updated LAI and z_0 values on a yearly basis. The model underestimates NO_3^- wet deposition, and NH_4^+ to a lesser extent, too. The modelled NH_3 surface concentrations are in general higher than observed concentrations. The opposite is true for NO_2, here, the modelled surface concentrations are lower than the observed concentrations. The computed measures did not change drastically due to the inclusion of the updated z_0 and LAI values. Of the two, the newly implemented MODIS LAI values seem to have a larger effect on both the NH_3 and NO_2 concentrations, leading to a slightly depreciated RMSE and slope for both NH_3 and NO_2.

Figure 16 shows the monthly mean NO_3^- wet deposition, NH_4^+ wet deposition, NH_3 surface concentration and NO_2 surface concentrations for the different model runs and the mean of the corresponding in situ observations. The relative changes with respect to the default model run are shown in the bottom figures. For NH_4^+, the model captures the observed pattern quite well, although the mean spring peak has slightly shifted. The model captures the monthly variation of NO_3^- well in general, too. There appears to be an underestimation during the winter, especially in December. The observed NH_3 surface concentrations are lower than the modelled concentrations at the beginning of spring and higher during summer. The measured NO_2 surface concentrations are continuously higher than the modelled values. A potential reason for this might be the spread of the NO_2 stations. Unlike NH_3, NO_2 is not only measured in nature areas but in all types of locations. Even the selected background stations may, therefore, be located relatively closer to emission sources, leading to higher observed NO_2 surface concentrations. The changes due to the inclusion of either the MODIS LAI or the updated z_0 values in our model are limited.

Both Table 5 and Figure 17 illustrate that the comparability of the modelled wet deposition and surface concentration fields to the available in-situ measurements did not change significantly. The impact of the updated LAI and z_0 values on these fields is largely an indirect effect of the more distinct changes in the dry deposition, and thus too small to lead to any drastic changes. We conclude that we are unable to demonstrate any major improvements with the use of the currently available in-situ measurements.

https://doi.org/10.5194/gmd-2019-256
Preprint. Discussion started: 1 October 2019

Geoscientific Model Development Discussions

5. Discussion

This paper aimed to improve the surface characterization of LOTOS-EUROS through the inclusion of satellite-derived leaf area index (LAI) and roughness length (z_0) values. We used empirical functions to derive roughness length (z_0) values for different land use classes. The updated z_0 values are compared to z_0 values from several studies (Wieringa, 1993;Silva et al., 2007;Troen and Petersen, 1989;Lankreijer et al., 1993;Yang and Friedl, 2003), and z_0 values used in other CTMs (Simpson et al., 2012;Bessagnet et al., 2017). Table 6 gives an overview of these z_0 values. There is in general good agreement with these z_0 values, and the updated z_0 values mostly fall within the stated ranges. The updated z_0 values for coniferous and deciduous forest are on the high side compared to these studies. These differences can in part be explained by the occurrence of relatively tall forest canopy (~30 meters) in the dataset, especially in forest in southern Germany, whereas most of these studies either assumed or studied shorter trees. Another possible explanation lies in the fact that we used a relatively large conversion factor of 0.136 (eq. 4), whereas a factor of 0.10 is also used quite often.

The updated z_0 values are linked to specific land use pixels and are therefore assumed reasonable estimates for moderately homogeneous areas with this specific land use type. There are various approaches to combine these z_0 values into an 'effective' roughness for larger, mixed areas (e.g. (Claussen, 1990;Mason, 1988)). The LOTOS-EUROS model uses logarithmic averaging to compute an effective roughness for an entire model pixel. This averaging step seems to be one of the reasons why the effect of our updated z_0 values on the deposition fields is limited. To illustrate this, the relative change in total dry NH_3 deposition due to the updated z_0 values were computed and shown in Figure 17. We used increasing threshold percentages to sort the NH_3 deposition on a model pixel level per land use type and fraction. Figure 17 shows that the differences in total NH_3 deposition between the two runs increase with increasing land use fraction. The model pixels that mostly consist of one type of land use seem to show the largest change in NH_3 deposition. The change thus appears to be less distinct in pixels that have a higher degree of mixing. Most of the model pixels largely contain mixtures of different land uses on the current model resolution. As a results, averaging of z_0 on a model pixel level is thus likely to cause a levelling effect on the current model resolution. The impact of the updated z_0 values is therefore expected to be larger at a higher model resolution. The use of another approach for computing the 'effective' roughness could potentially lead to stronger changes in the modelled deposition fields. Here, however, we merely focus on updating the z_0 values per land use, and we consider the effect of this beyond the scope of this paper.

Moreover, we should also consider the limitations of the datasets used in this study. The previous versions of the MODIS-LAI have been validated in many studies (e.g. (Fang et al., 2012;Wang et al., 2004;Kobayashi et al., 2010)), showing an overall good agreement with ground observed LAI values and other LAI products. The seasonality in LAI is properly captured for most biomes, but unrealistic temporal variability is observed for forest due to infrequent observations. Also, the previous versions overestimate LAI for forests (Fang et al., 2012;Kobayashi et al., 2010;Wang et al., 2004). Although the MODIS-LAI products have been gradually improving with each update, these issues still exist in the newer versions of the product. For the most recent version of the MODIS-LAI, version 6, Yan et al. (2016) found an overall RMSE of 0.66 and a R^2 of 0.77 in comparison with LAI ground observation.

https://doi.org/10.5194/gmd-2019-256
Preprint. Discussion started: 1 October 2019

Geoscientific Model Development Discussions

More recently, using a different approach, Xu et al. (2018) found a slightly higher RMSE of 0.93 and a R^2 of 0.77. The overestimation of high LAI values for forests could potentially have led to an overestimated dry deposition velocity, and herewith overestimated N_r deposition, for deciduous and coniferous forests in this study. The forest canopy height map used in this study has been validated against 66 FLUXNET sites (Simard et al., 2011). The results showed that RMSE = 4.4 m and R^2 = 0.7 after removal of 7 outliers. Although this dataset has a strong correlation with in situ observations, our method could potentially be improved by using another product with either a higher precision or resolution. For modelling studies on a national level one could or instance consider the use of airborne LiDAR point clouds to retrieve forest canopy heights. This procedure, although it is computationally expensive, would allow us to create high resolution z_0 maps.

The inclusion of the MODIS-LAI led to a more accurate spatial and temporal distribution of LAI values. Also, the updated, time-variant z_0 values give a more realistic representation of the growing season due to their dependency on both the NDVI and LAI. Moreover, we included canopy height dependent z_0 values for forests. The obtained z_0 values for forests now have a spatial variation and we can observe a latitudinal gradient with increasing z_0 values towards the south of Germany.

We evaluated the effect of updated z_0 and LAI values on modelled N_r distribution and deposition fields. The total terrestrial N_r deposition on a country level did not change drastically, with a maximum increase of ~6.2% in Belgium due to the inclusion of the relatively higher MODIS-LAI values. The distribution of the relative changes in deposition of the reduced and oxidized forms of reactive nitrogen showed a similar pattern. Here, the updated z_0 values led to a variation of ~±8%, and the updated LAI values led to variations of ~±30% in both fields. The most distinct effect can be observed in the dry deposition fields. These fields varied from approximately -20% to +20% with the updated z_0 map, and from -20% even up to +30% with the MODIS LAI values. As a result, we observed a shift from wet to dry deposition, except for the Netherlands, where we observe an opposite shift, from dry to wet deposition. Moreover, we observed a redistribution of N_r deposition over different land use classes on a sub grid level. To illustrate the potential consequences on a local scale, we computed the critical load exceedances for deciduous and coniferous forest (Figure 17) using critical loads of 10 kg following Bobbink et al. (2010b). Compared to the default run, the changes may be sizable locally, ranging from approximately -3 kg up to +2 kg for deciduous forest and even over -3 kg for coniferous forest.

We showed that the corresponding modelled NH_3 surface concentrations may vary up to ~10% locally due to updated z_0 and LAI values, and the NO_2 surface concentrations up to approximately -5%. We compared the outputs from the different runs to available in-situ observations. The changes in modelled NH_3 and NO_2 surface concentration and NH_4^+ and NO_3^- wet deposition due to the inclusion of the updated z_0 and LAI values were, however, relatively small. As a result, we were not able to identify significant improvements in the comparability with in-situ measurements.

This work has shown that changes in two of the main deposition parameters (LAI, z_0) can already lead to distinct changes (~30%) in the modelled deposition fields. This demonstrates the model's sensitivity toward these input

https://doi.org/10.5194/gmd-2019-256
Preprint. Discussion started: 1 October 2019

values, especially the LAI. In addition to the known uncertainty involved with surface exchange parameterization itself, this further stresses the need for further research. Another important aspect that should receive more attention is the validation of the dry deposition fields with in-situ dry deposition measurements. Here we illustrated the need for direct validation methods, as relatively large changes in modelled dry deposition field cannot be verified sufficiently by surface concentration and wet deposition measurements.

The surface-atmosphere exchange remains one of the most important uncertainties in deposition modelling. The use of satellite products to derive LAI and z_0 values is, in our view, an initial step toward a more accurate representation of the surface characterization in models, that might help us to minimize the uncertainty in deposition modelling. The approach to derive high resolution, dynamic z_0 estimates presented here can be linked to any land use map and is as such transferable to many different models and geographical areas.

Data availability. LOTOS-EUROS is open source and can be downloaded from https://lotos-euros.tno.nl/.

Author Contribution. JWE, MS and SG designed the research. RK, AS and SG performed the model simulations. SG did the input data processing and model output analysis. All authors contributed to the interpretation of the results. SG wrote the paper with contributions from all co-authors.

Competing interests. The authors declare that they have no conflict of interest.

References

Abida, R., Attié, J.-L., El Amraoui, L., Lahoz, W. A., Ricaud, P., Eskes, H., Segers, A., Curier, L., de Haan, J., and Kujanpää, J.: Impact of spaceborne carbon monoxide observations from the S-5P platform on tropospheric composition analyses and forecasts, 2017.

Bauer, S. E., Tsigaridis, K., and Miller, R.: Significant atmospheric aerosol pollution caused by world food cultivation, Geophys Res Lett, 43, 5394-5400, 2016.

Behera, S. N., Sharma, M., Aneja, V. P., and Balasubramanian, R.: Ammonia in the atmosphere: a review on emission sources, atmospheric chemistry and deposition on terrestrial bodies, Environmental Science and Pollution Research, 20, 8092-8131, 2013.

Bessagnet, B., Khvorostyanov, D., Menut, L., Monge, J., and Vautard, R.: Documentaion of the chemistry transport model CHIMERE, Institute Pierre Simon Laplace, INERIS, LISA, 260, 2017.

Bobbink, R., Hicks, K., Galloway, J., Spranger, T., Alkemade, R., Ashmore, M., Bustamante, M., Cinderby, S., Davidson, E., and Dentener, F.: Global assessment of nitrogen deposition effects on terrestrial plant diversity: a synthesis, Ecol Appl, 20, 30-59, 2010a.

Bobbink, R., Hicks, K., Galloway, J., Spranger, T., Alkemade, R., Ashmore, M., Bustamante, M., Cinderby, S., Davidson, E., Dentener, F., Emmett, B., Erisman, J. W., Fenn, M., Gilliam, F., Nordin, A., Pardo, L., and De Vries, W.: Global assessment of nitrogen deposition effects on terrestrial plant diversity: a synthesis, Ecol Appl, 20, 30-59, Doi 10.1890/08-1140.1, 2010b.

Bolle, H., and Streckenbach, B.: Flux estimates from remote sensing, The Echival Field Experiment in a Desertification Threatened Area (EFEDA), final report, 406-424, 1993.

https://doi.org/10.5194/gmd-2019-256
Preprint. Discussion started: 1 October 2019

Geoscientific Model Development Discussions

Brutsaert, W.: Evaporation into the atmosphere: theory, history and applications, Springer Science & Business Media, 2013.

Businger, J. A., Wyngaard, J. C., Izumi, Y., and Bradley, E. F.: Flux-profile relationships in the atmospheric surface layer, Journal of the atmospheric Sciences, 28, 181-189, 1971.

Butterbach-Bahl, K., Nemitz, E., Zaehle, S., Billen, G., Boeckx, P., Erisman, J. W., Garnier, J., Upstill-Goddard, R., Kreuzer, M., and Oenema, O.: Nitrogen as a threat to the European greenhouse balance, 2011.

Claussen, M.: Area-averaging of surface fluxes in a neutrally stratified, horizontally inhomogeneous atmospheric boundary-layer, Atmos Environ a-Gen, 24, 1349-1360, 1990.

Colette, A., Andersson, C., Manders, A., Mar, K., Mircea, M., Pay, M., Raffort, V., Tsyro, S., Cuvelier, C., and Adani, M.: EURODELTA-Trends, a multi-model experiment of air quality hindcast in Europe over 1990–2010, Geosci. Model Dev., 10, 3255–3276. 2017.

Curier, R., Kranenburg, R., Segers, A., Timmermans, R., and Schaap, M.: Synergistic use of OMI NO2 tropospheric columns and LOTOS–EUROS to evaluate the NOx emission trends across Europe, Remote Sens Environ, 149, 58-69, 2014.

Davi, H., Soudani, K., Deckx, T., Dufrene, E., Le Dantec, V., and Francois, C.: Estimation of forest leaf area index from SPOT imagery using NDVI distribution over forest stands, Int J Remote Sens, 27, 885-902, 2006.

Didan, K.: MYD13A3 MODIS/Aqua Vegetation Indices Monthly L3 Global 1km SIN Grid V006, NASA EOSDIS LP DAAC, 10.5067/MODIS/MYD13A3.006, 2015.

Emberson, L., Simpson, D., Tuovinen, J., Ashmore, M., and Cambridge, H.: Towards a model of ozone deposition and stomatal uptake over Europe, EMEP MSC-W Note, 6, 1-57, 2000.

EMEP: The European Monitoring and Evaluation Programme EMEP Status Report, 2016.

Erisman, J., and Schaap, M.: The need for ammonia abatement with respect to secondary PM reductions in Europe, Environ Pollut, 129, 159-163, 2004.

Erisman, J. W., Van Pul, A., and Wyers, P.: Parametrization of surface resistance for the quantification of atmospheric deposition of acidifying pollutants and ozone, Atmos Environ, 28, 2595-2607, 1994.

Erisman, J. W., Galloway, J., Seitzinger, S., Bleeker, A., and Butterbach-Bahl, K.: Reactive nitrogen in the environment and its effect on climate change, Curr Opin Env Sust, 3, 281-290, 2011.

European Centre for Medium-Range Weather Forecasts: Annual report, 2016.

European Environmental Agency: CLC2012 Addendum to CLC2006 Technical Guidelines, EEA Report, 2014.

European Environmental Agency: Airbase dataset, http://discomap.eea.europa.eu, 2019.

Fang, H., Wei, S., and Liang, S.: Validation of MODIS and CYCLOPES LAI products using global field measurement data, Remote Sens Environ, 119, 43-54, 2012.

Fowler, D., Steadman, C. E., Stevenson, D., Coyle, M., Rees, R. M., Skiba, U., Sutton, M., Cape, J., Dore, A., and Vieno, M.: Effects of global change during the 21st century on the nitrogen cycle, Atmos Chem Phys, 15, 13849-13893, 2015.

https://doi.org/10.5194/gmd-2019-256
Preprint. Discussion started: 1 October 2019

Geoscientific Model Development Discussions

Gallagher, M., Nemitz, E., Dorsey, J., Fowler, D., Sutton, M., Flynn, M., and Duyzer, J.: Measurements and parameterizations of small aerosol deposition velocities to grassland, arable crops, and forest: Influence of surface roughness length on deposition, Journal of Geophysical Research: Atmospheres, 107, 2002.

Gallego, F. J.: A population density grid of the European Union, Population and Environment, 31, 460-473, 2010.

Galloway, J. N., Aber, J. D., Erisman, J. W., Seitzinger, S. P., Howarth, R. W., Cowling, E. B., and Cosby, B. J.: The nitrogen cascade, AIBS Bulletin, 53, 341-356, 2003.

Galloway, J. N., Dentener, F. J., Capone, D. G., Boyer, E. W., Howarth, R. W., Seitzinger, S. P., Asner, G. P., Cleveland, C. C., Green, P., and Holland, E. A.: Nitrogen cycles: past, present, and future, Biogeochemistry, 70, 153-226, 2004.

Galloway, J. N., Townsend, A. R., Erisman, J. W., Bekunda, M., Cai, Z. C., Freney, J. R., Martinelli, L. A., Seitzinger, S. P., and Sutton, M. A.: Transformation of the nitrogen cycle: Recent trends, questions, and potential solutions, Science, 320, 889-892, 10.1126/science.1136674, 2008.

Hatfield, J.: Large scale evapotranspiration from remotely sensed surface temperature, Planning Now for Irrigation and Drainage in the 21st Century, 1988, 502-509,

Hendriks, C., Kranenburg, R., Kuenen, J. J. P., Van den Bril, B., Verguts, V., and Schaap, M.: Ammonia emission time profiles based on manure transport data improve ammonia modelling across north western Europe, Atmos Environ, 131, 83-96, 10.1016/j.atmosenv.2016.01.043, 2016.

Houborg, R., and Boegh, E.: Mapping leaf chlorophyll and leaf area index using inverse and forward canopy reflectance modeling and SPOT reflectance data, Remote Sens Environ, 112, 186-202, 2008.

Jonckheere, I., Fleck, S., Nackaerts, K., Muys, B., Coppin, P., Weiss, M., and Baret, F.: Review of methods for in situ leaf area index determination: Part I. Theories, sensors and hemispherical photography, Agr Forest Meteorol, 121, 19-35, 2004.

Kobayashi, H., Delbart, N., Suzuki, R., and Kushida, K.: A satellite-based method for monitoring seasonality in the overstory leaf area index of Siberian larch forest, Journal of Geophysical Research: Biogeosciences, 115, 2010.

Kuenen, J. J. P., Visschedijk, A. J. H., Jozwicka, M., and van der Gon, H. A. C. D.: TNO-MACC_II emission inventory; a multi-year (2003-2009) consistent high-resolution European emission inventory for air quality modelling, Atmos Chem Phys, 14, 10963-10976, 10.5194/acp-14-10963-2014, 2014.

Lankreijer, H., Hendriks, M., and Klaassen, W.: A comparison of models simulating rainfall interception of forests, Agr Forest Meteorol, 64, 187-199, 1993.

Lelieveld, J., Evans, J. S., Fnais, M., Giannadaki, D., and Pozzer, A.: The contribution of outdoor air pollution sources to premature mortality on a global scale, Nature, 525, 367, 2015.

Lolkema, D. E., Noordijk, H., Stolk, A. P., Hoogerbrugge, R., van Zanten, M. C., and van Pul, W. A. J.: The Measuring Ammonia in Nature (MAN) network in the Netherlands, Biogeosciences, 12, 5133-5142, 10.5194/bg-12-5133-2015, 2015.

Manders-Groot, A., Segers, A., Jonkers, S., Schaap, M., Timmermans, R., Hendriks, C., Sauter, F., Kruit, R. W., van der Swaluw, E., and Eskes, H.: LOTOS-EUROS v2. 0 reference guide, TNO report TNO2016, 10898, 2016.

Manders, A. M. M., Builtjes, P. J. H., Curier, L., Denier van der Gon, H. A. C., Hendriks, C., Jonkers, S., Kranenburg, R., Kuenen, J., Segers, A. J., Timmermans, R. M. A., Visschedijk, A., Wichink Kruit, R. J., Van Pul, W. A. J., Sauter, F. J., van der Swaluw, E., Swart, D. P. J., Douros, J., Eskes, H., van Meijgaard, E., van Ulft, B., van Velthoven, P., Banzhaf, S., Mues, A., Stern, R., Fu, G., Lu, S., Heemink, A., van Velzen, N., and Schaap, M.:

https://doi.org/10.5194/gmd-2019-256
Preprint. Discussion started: 1 October 2019

Geoscientific Model Development Discussions

Curriculum vitae of the LOTOS–EUROS (v2.0) chemistry transport model, Geosci Model Dev, 10(11), 10.5194/gmd-10-4145-2017, 2017.

Mason, P.: The formation of areally-averaged roughness lengths, Q J Roy Meteor Soc, 114, 399-420, 1988.

McNaughton, K. G., and Van Den Hurk, B. J. J. M.: A 'Lagrangian' revision of the resistors in the two-layer model for calculating the energy budget of a plant canopy, Bound-Lay Meteorol, 74, 261-288, 10.1007/bf00712121, 1995.

Moran, M. S.: A satellite-based approach for evaluation of the spatial distribution of evapotranspiration from agricultural lands, 1990.

Myneni, R., Knyazikhin, Y., and Park, T.: MCD15A2H MODIS/Terra+Aqua Leaf Area Index/FPAR 8-day L4 Global 500m SIN Grid V006, NASA EOSDIS Land Processes DAAC, 10.5067/MODIS/MCD15A2H.006, 2015.

Nakai, T.: Parameterisation of aerodynamic roughness over boreal, cool-and warm-temperate forests, Agr Forest Meteorol, 148, 1916, 2008.

Paerl, H. W., Gardner, W. S., McCarthy, M. J., Peierls, B. L., and Wilhelm, S. W.: Algal blooms: noteworthy nitrogen, Science, 346, 175-175, 2014.

Plate, E. J.: Aerodynamic Characteristics of Atmospheric Boundary Layers, Argonne National Lab., Ill. Karlsruhe Univ.(West Germany), 1971.

Raupach, M.: Simplified expressions for vegetation roughness length and zero-plane displacement as functions of canopy height and area index, Bound-Lay Meteorol, 71, 211-216, 1994.

Reis, S., Pinder, R., Zhang, M., Lijie, G., and Sutton, M.: Reactive nitrogen in atmospheric emission inventories, Atmos Chem Phys, 9, 7657-7677, 2009.

Schaap, M., Manders, A., Hendricks, J. M., Cnossen, A. J. S., Segers, H. A. C., Denier van der Gon, M., Jozwicka, M., Sauter, F., Velders, G., Matthijsen, J., and Builtjes, P.: Regional modelling of particulate matter for the Netherlands, Netherlands Research Program on Particulate Matter, 500099008, 2009.

Schaap, M., Banzhaf, S., Scheuschner, T., Geupel, M., Hendriks, C., Kranenburg, R. and Builtjes, P. J. H. : Atmospheric nitrogen deposition to terrestrial ecosystems across Germany, Biogeosciences, in review, 2019.

Schaudt, K., and Dickinson, R.: An approach to deriving roughness length and zero-plane displacement height from satellite data, prototyped with BOREAS data, Agr Forest Meteorol, 104, 143-155, 2000.

Schrader, F., and Brummer, C.: Land Use Specific Ammonia Deposition Velocities: a Review of Recent Studies (2004-2013), Water Air Soil Poll, 225, ARTN 2114 10.1007/s11270-014-2114-7, 2014.

Schrader, F., Brummer, C., Flechard, C. R., Kruit, R. J. W., van Zanten, M. C., Zoll, U., Hensen, A., and Erisman, J. W.: Non-stomatal exchange in ammonia dry deposition models: comparison of two state-of-the-art approaches, Atmos Chem Phys, 16, 13417-13430, 10.5194/acp-16-13417-2016, 2016.

Silva, J., Ribeiro, C., and Guedes, R.: Roughness length classification of Corine Land Cover classes, Proceedings of the European Wind Energy Conference, Milan, Italy, 2007, 110,

Simard, M., Pinto, N., Fisher, J. B., and Baccini, A.: Mapping forest canopy height globally with spaceborne lidar, Journal of Geophysical Research: Biogeosciences, 116, 2011.

Simpson, D., Benedictow, A., Berge, H., Bergström, R., Emberson, L. D., Fagerli, H., Flechard, C. R., Hayman, G. D., Gauss, M., Jonson, J. E., Jenkin, M. E., Nyíri, A., Richter, C., Semeena, V. S., Tsyro, S., Tuovinen, J. P.,

https://doi.org/10.5194/gmd-2019-256
Preprint. Discussion started: 1 October 2019

Geoscientific Model Development Discussions

Valdebenito, Á., and Wind, P.: The EMEP MSC-W chemical transport model – technical description, Atmos. Chem. Phys., 12, 7825-7865, 10.5194/acp-12-7825-2012, 2012.

Skjøth, C. A., Geels, C., Berge, H., Gyldenkærne, S., Fagerli, H., Ellermann, T., Frohn, L. M., Christensen, J., Hansen, K. M., Hansen, K., and Hertel, O.: Spatial and temporal variation in ammonia emissions - a freely accessible model code for Europe Atmos Chem Phys, 11, 5221-5236, 10.5194/acp-11-5221-2011, 2011.

Soudani, K., François, C., Le Maire, G., Le Dantec, V., and Dufrêne, E.: Comparative analysis of IKONOS, SPOT, and ETM+ data for leaf area index estimation in temperate coniferous and deciduous forest stands, Remote Sens Environ, 102, 161-175, 2006.

Troen, I., and Petersen, E. L.: European wind atlas. Risø national laboratory, Roskilde, Weibull W.(1951). A statistical distribution function of wide applicability. J. Appl. mech, 18, 293-297, 1989.

Turner, D. P., Cohen, W. B., Kennedy, R. E., Fassnacht, K. S., and Briggs, J. M.: Relationships between leaf area index and Landsat TM spectral vegetation indices across three temperate zone sites, Remote Sens Environ, 70, 52-68, 1999.

Van Zanten, M., Kruit, R. W., Hoogerbrugge, R., Van der Swaluw, E., and Van Pul, W.: Trends in ammonia measurements in the Netherlands over the period 1993–2014, Atmos Environ, 148, 352-360, 2017.

van Zanten, M. C., Sauter, F. J., Wichink Kruit, R. J., van Jaarsveld, J. A., and van Pul, M. A. J.: Description of the DEPAC module: Dry deposition modelling with DEPAC_GCN2010, Rivm Report 680180001/2010, RIVM, Bilthoven, Netherlands, 2010.

Wang, Y., Woodcock, C. E., Buermann, W., Stenberg, P., Voipio, P., Smolander, H., Häme, T., Tian, Y., Hu, J., and Knyazikhin, Y.: Evaluation of the MODIS LAI algorithm at a coniferous forest site in Finland, Remote Sens Environ, 91, 114-127, 2004.

Watson, D. J.: Comparative physiological studies on the growth of field crops: I. Variation in net assimilation rate and leaf area between species and varieties, and within and between years, Annals of botany, 11, 41-76, 1947.

Wesely, M.: Parameterization of surface resistances to gaseous dry deposition in regional-scale numerical models, Atmospheric Environment (1967), 23, 1293-1304, 1989.

Wichink Kruit, R. J., Schaap, M., Sauter, F. J., van Zanten, M. C., and van Pul, W. A. J.: Modeling the distribution of ammonia across Europe including bi-directional surface-atmosphere exchange, Biogeosciences, 9, 5261-5277, 10.5194/bg-9-5261-2012, 2012.

Wieringa, J.: Representative roughness parameters for homogeneous terrain, Bound-Lay Meteorol, 63, 323-363, 1993.

Wu, Z., Schwede, D. B., Vet, R., Walker, J. T., Shaw, M., Staebler, R., and Zhang, L.: Evaluation and intercomparison of five North American dry deposition algorithms at a mixed forest site, Journal of Advances in Modeling Earth Systems, 10, 1571-1586, 2018.

Xing, Q., Wu, B., Yan, N., Yu, M., and Zhu, W.: Evaluating the relationship between field aerodynamic roughness and the MODIS BRDF, NDVI, and wind speed over grassland, Atmosphere, 8, 16, 2017.

Xu, B., Li, J., Park, T., Liu, Q., Zeng, Y., Yin, G., Zhao, J., Fan, W., Yang, L., and Knyazikhin, Y.: An integrated method for validating long-term leaf area index products using global networks of site-based measurements, Remote Sens Environ, 209, 134-151, 2018.

https://doi.org/10.5194/gmd-2019-256
Preprint. Discussion started: 1 October 2019

Geoscientific Model Development Discussions

Yan, K., Park, T., Yan, G., Liu, Z., Yang, B., Chen, C., Nemani, R. R., Knyazikhin, Y., and Myneni, R. B.: Evaluation of MODIS LAI/FPAR product collection 6. Part 2: Validation and intercomparison, Remote Sensing, 8, 460, 2016.

Yang, R., and Friedl, M. A.: Determination of roughness lengths for heat and momentum over boreal forests, Bound-Lay Meteorol, 107, 581-603, 2003.

Yu, M., Wu, B., Yan, N., Xing, Q., and Zhu, W.: A method for estimating the aerodynamic roughness length with NDVI and BRDF signatures using multi-temporal Proba-V data, Remote Sensing, 9, 6, 2016.

Zwally, H., Schutz, B., Abdalati, W., Abshire, J., Bentley, C., Brenner, A., Bufton, J., Dezio, J., Hancock, D., and Harding, D.: ICESat's laser measurements of polar ice, atmosphere, ocean, and land, Journal of Geodynamics, 34, 405-445, 2002.

DEPAC class	Dataset
1 - Grass	MODIS NDVI
2 - Arable land	MODIS NDVI
3 - Permanent crops	MODIS NDVI
4 - Coniferous forest	GLAS forest canopy height
5 - Deciduous forest	GLAS forest canopy height, MODIS LAI
6 - Water	-
7 - Urban	Population density
8 - Other	MODIS NDVI
9 - Desert	-

Table 1: An overview of the datasets that are used to derive z_0 input values for each DEPAC land use category.

Function		Vegetation type(s)	Reference
$z_0 = \begin{cases} -0.173 + 1.168 * NDVI - 1.125 * NDVI^2 & \text{for NDVI} < 0.6 \\ 0.1 & \text{for NDVI} \geq 0.6 \end{cases}$	(eq. 6)	Partial cover cotton and wheat canopies	Hatfield (1988)
$z_0 = e^{-5.2+5.3*NDVI}$	(eq. 7)	Alfalfa (Arizona)	Moran (1990)
$z_0 = e^{-5.5+5.8*NDVI}$	(eq. 8)	Mixed, non-irrigated agricultural land (Mediterranean)	Bolle and Streckenbach (1993)
$z_0 = 0.2255 * NDVI + 0.0087$	(eq. 9)	Spring maize	Yu et al. (2016)
$z_0 = 0.2476 * NDVI + 0.0615$	(eq. 10)	Winter wheat	Yu et al. (2016)
$z_0 = 0.2858 * NDVI + 0.1017$	(eq. 11)	Summer maize	Yu et al. (2016) Xing et al. (2017)
$z_0 = 0.0203 * NDVI^{0.9547}$	(eq. 12)	Grassland	

Table 2: Studies that relate the aerodynamic roughness length (z_0) to satellite-derived NDVI values for specific land cover types and conditions.

https://doi.org/10.5194/gmd-2019-256
Preprint. Discussion started: 1 October 2019

Geoscientific Model Development Discussions

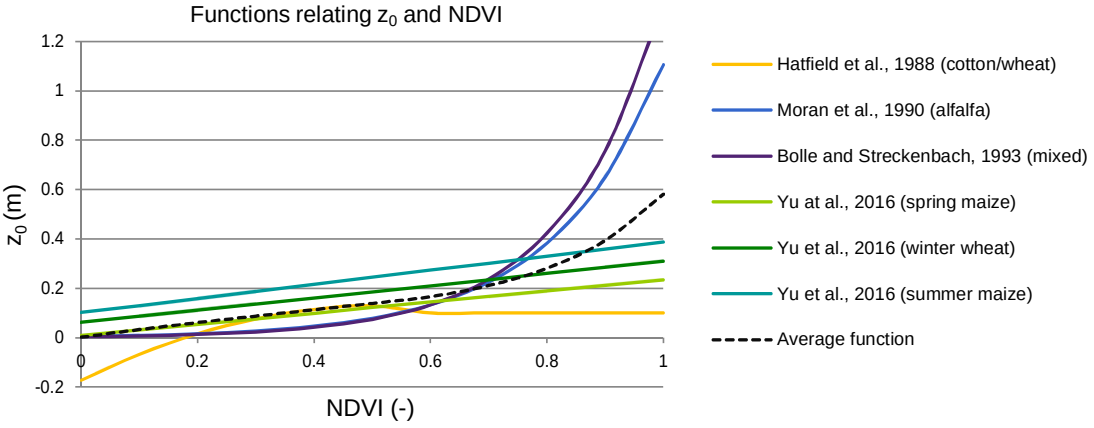

Figure 1: Several functions that relate the roughness length, z_0 (m) to the normalized difference vegetation index (NDVI). The dotted line shows the average of all the functions. This function is used to compute NDVI-dependent z_0 values for the subcategories within DEPAC classes "arable", "other" and "permanent crops".

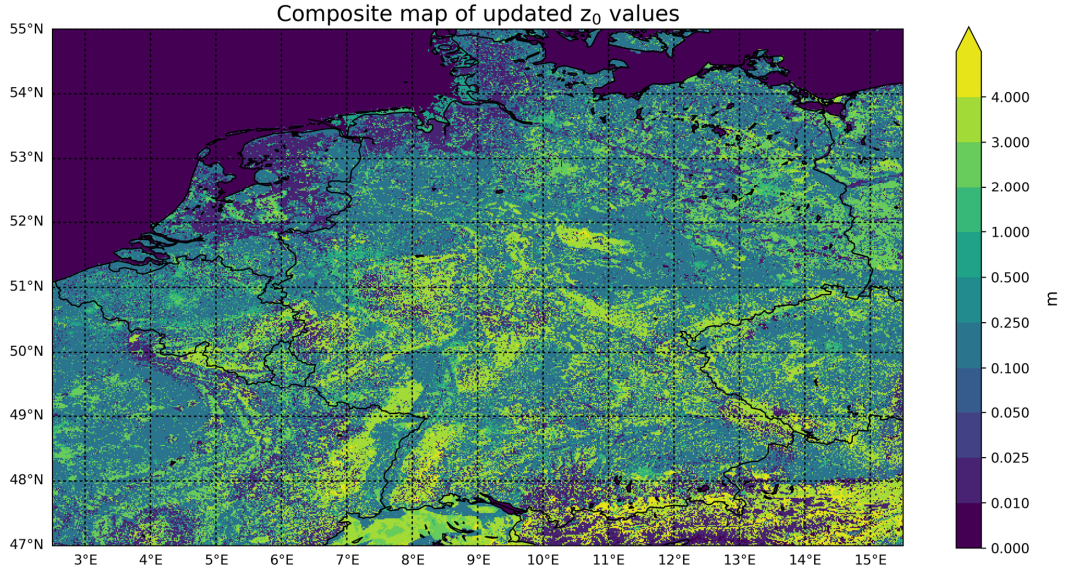

Figure 2: Composite map of the new z_0 values. The yearly mean is displayed for land use classes with time-variant z_0 values.

https://doi.org/10.5194/gmd-2019-256
Preprint. Discussion started: 1 October 2019

Geoscientific Model Development Discussions

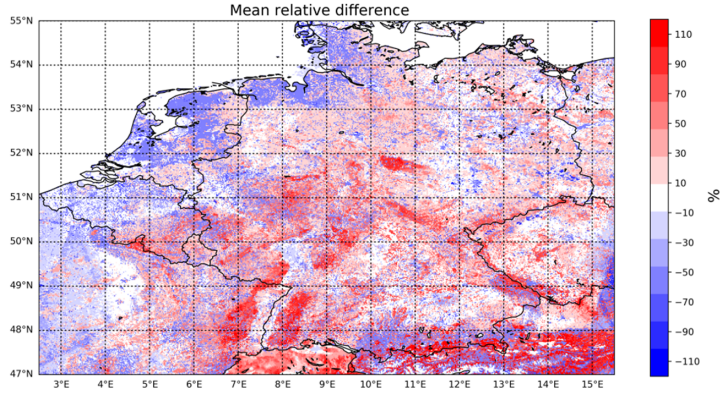

640

Figure 3: Mean relative difference (%) of the updated z_0 values with respect to the default z_0 values.

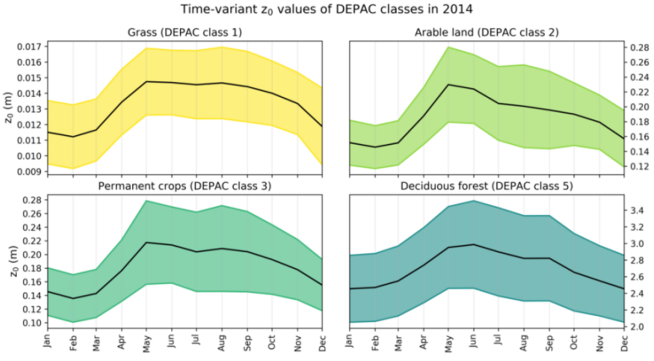

Figure 4: Yearly variation of the updated z_0 values per DEPAC class. The black line represents the mean z_0 of all pixels within the modelled grid for that particular DEPAC class, the ranges represent the mean z_0 plus and minus the standard deviation of z_0.

645

DEPAC class	Default z_0	New mean z_0 (σ)
1 - Grass	0.03	0.013 (0.002)
2 - Arable land	0.1	0.19 (0.04)
3 - Permanent crops	0.25	0.20 (0.04)
4 - Coniferous forest	2	2.91 (0.56)
5 - Deciduous forest	2	2.55 (0.51)
6 - Water	0.002	-
7 - Urban	2	0.92 (0.20)
8 - Other	0.05	0.19 (0.05)
9 - Desert	0.013	-

Table 3: An overview of the default and the adjusted roughness length of each DEPAC class used in LOTOS-EUROS for Germany, the Netherlands and Belgium. The datasets that are used to derive the updated z_0 values are given in the last column. The mean z_0 value of the DEPAC classes computed using the MODIS NDVI product is the yearly mean of all monthly z_0 values.

https://doi.org/10.5194/gmd-2019-256
Preprint. Discussion started: 1 October 2019

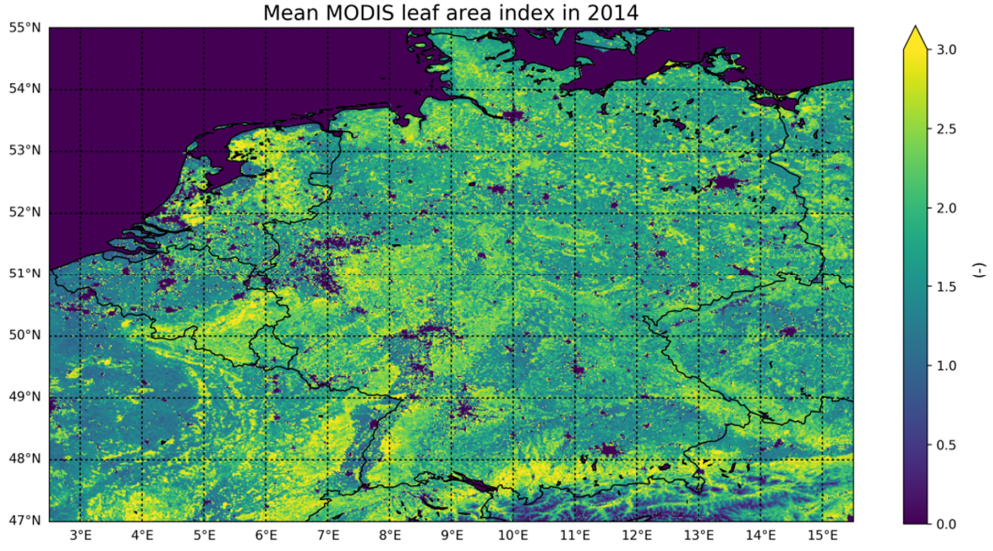

650

Figure 5: The yearly mean MODIS leaf area index in 2014.

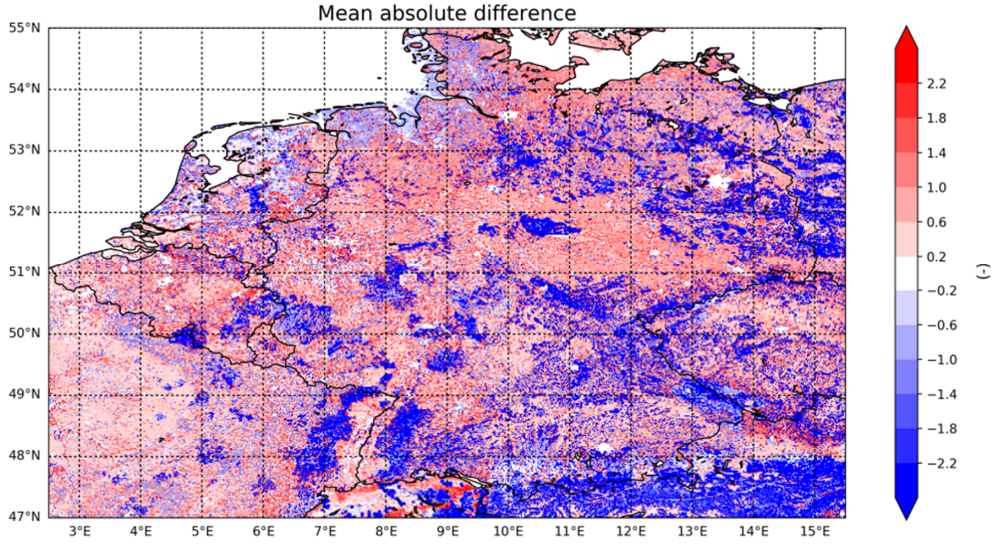

Figure 6: The absolute differences ($LAI_{MODIS} - LAI_{default}$) between the MODIS leaf area index and the default leaf area index in LOTOS-EUROS.

https://doi.org/10.5194/gmd-2019-256
Preprint. Discussion started: 1 October 2019

Geoscientific Model Development Discussions

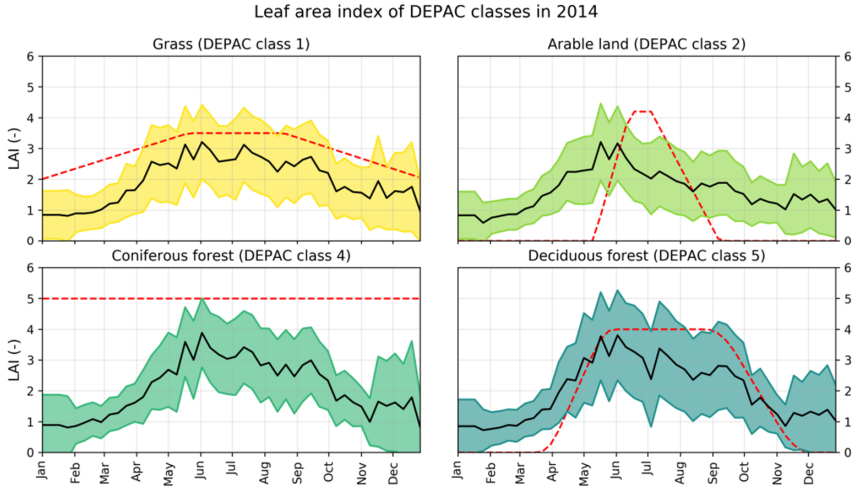

Figure 7: Yearly variation of the default and MODIS-LAI values per DEPAC class. The black line represents the mean MODIS-LAI of all pixels within the modelled grid for that particular DEPAC class, the ranges represent the mean plus and minus the standard deviation of the MODIS-LAI. The red line depicts the default LAI values in LOTOS-EUROS.

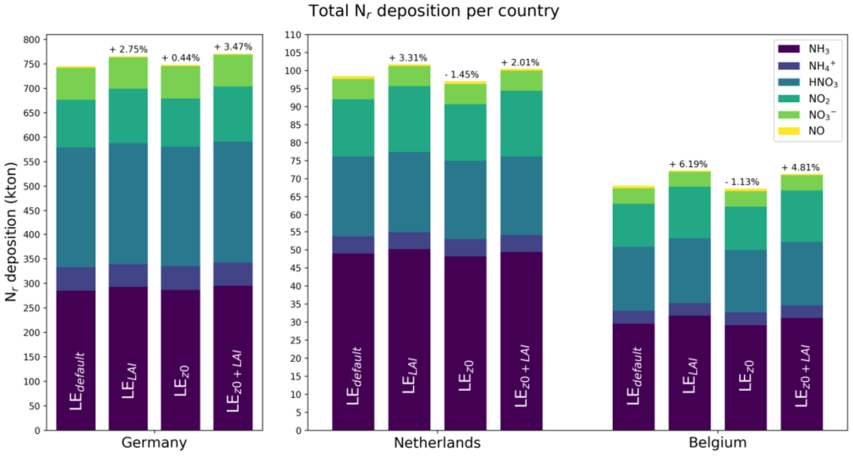

Figure 8: The total N_r deposition (kton) per country for each of the model runs, and the division into different N_r component. The colours depict the part of the total deposition each individual N_r component comprises. The numbers above the individual bars indicate the change in the total N_r deposition for each of the runs.

https://doi.org/10.5194/gmd-2019-256
Preprint. Discussion started: 1 October 2019

Geoscientific Model Development Discussions

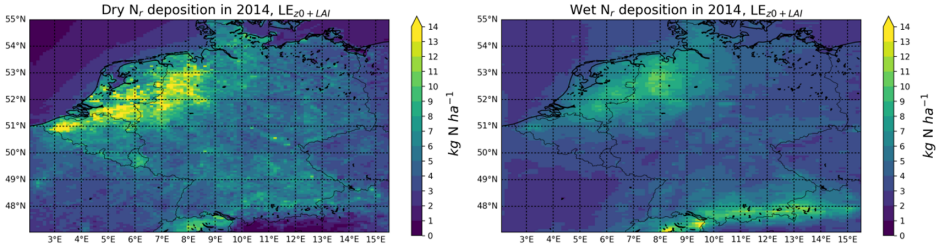

Figure 9: The modelled amount of dry (left) and wet (right) deposition in kg N ha^{-1} in 2014.

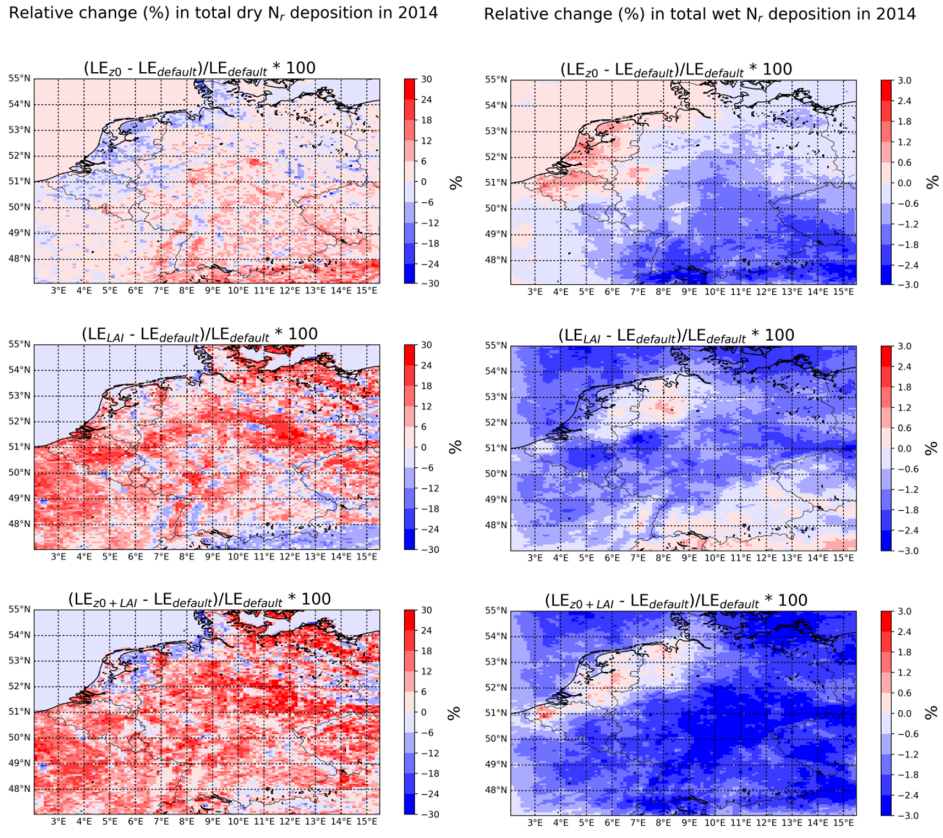

Figure 10: The relative change in total dry (left) and wet (right) N$_r$ deposition in 2014 for the different model runs relative to the default LOTOS-EUROS run. The first row indicates the changes related to the implementation of the updated z_0 values. The second row indicates the changes related to the implementation of the MODIS LAI values. The third row shows the combined effect of both these updates. (Please note the different scales).

https://doi.org/10.5194/gmd-2019-256
Preprint. Discussion started: 1 October 2019

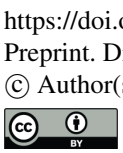

Geoscientific Model Development Discussions

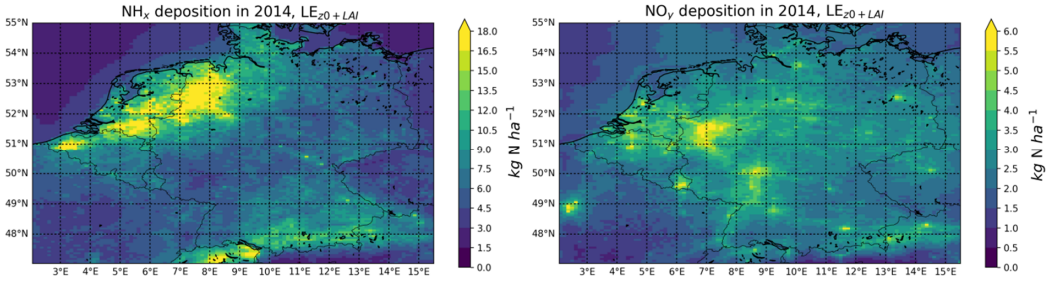

Figure 11: NH_x deposition (left) and NO_y deposition (right) in kg N ha^{-1} in 2014.

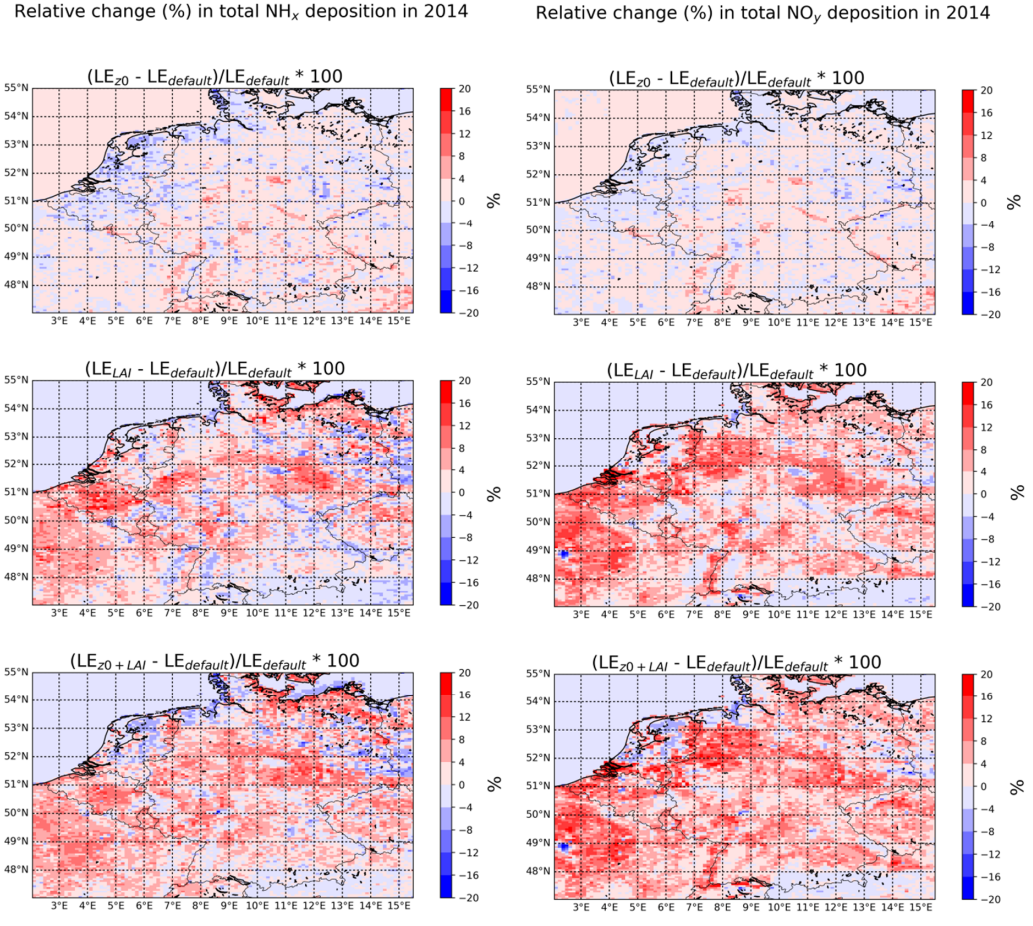

675

Figure 12: The relative change in total NH_x (top) and NO_y (bottom) deposition in 2014 for the different model runs relative to the default LOTOS-EUROS run. The first row indicates the changes related to the implementation of the updated z_0 values. The second row indicates the changes related to the implementation of the MODIS LAI values. The third row shows the combined effect of both these updates.

https://doi.org/10.5194/gmd-2019-256
Preprint. Discussion started: 1 October 2019

Geoscientific Model Development Discussions

	LE_{LAI}	LE_{z0}	LE_{z0+LAI}
Grass (1)	-5.34	-3.95	-8.05
Arable land (2)	9.53	3.27	12.88
Permanent crops (3)	0.22	-3.17	-2.78
Coniferous forest (4)	-9.36	-0.86	-7.36
Deciduous forest (5)	1.15	1.93	1.83
Urban (7)	16.62	-0.37	6.53
Other (6,8,9)	3.45	0.58	3.31

680

Table 4: Relative change (%) in total N_r deposition w.r.t. the default run over Germany, the Netherlands and Belgium in 2014 per land use class.

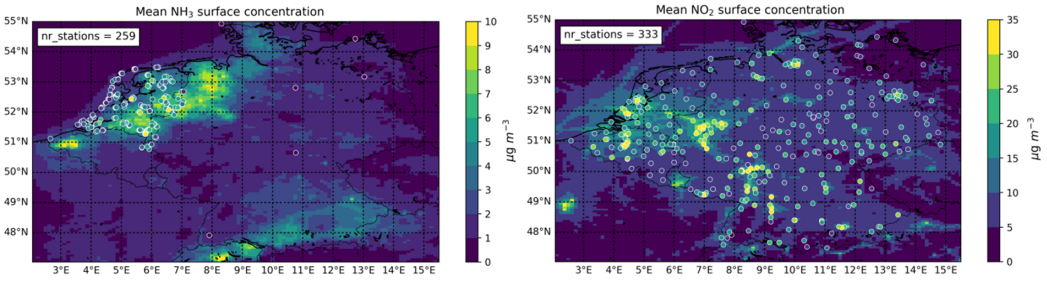

685 **Figure 13: The yearly mean NH_3 (left) and NO_2 (right) surface concentrations in µg m^{-3} in 2014, and the corresponding mean surface concentrations measured at the in-situ stations.**

https://doi.org/10.5194/gmd-2019-256
Preprint. Discussion started: 1 October 2019

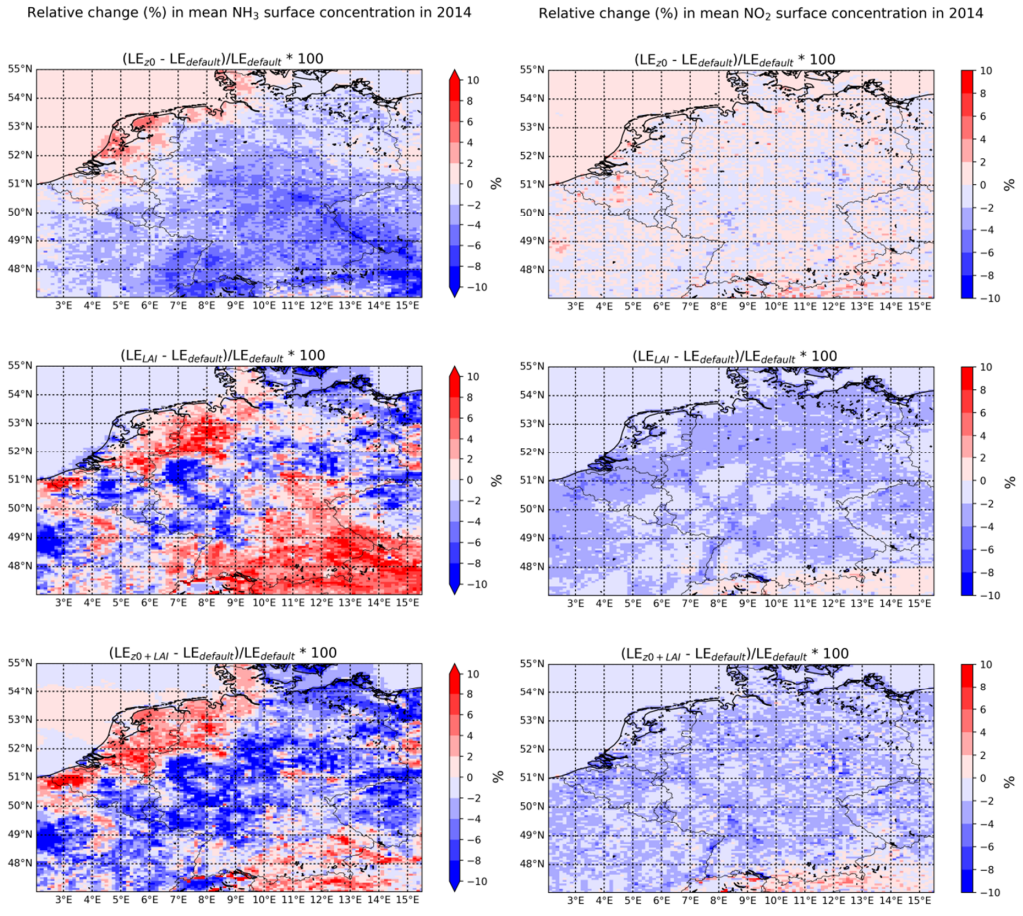

Figure 14: The relative change (%) in mean NH_3 (left) and NO_2 (right) surface concentration in 2014 for the different model runs relative to the default LOTOS-EUROS run. The first row indicates the changes related to the implementation of the updated z_0 values. The second row indicates the changes related to the implementation of the MODIS LAI values. The third row shows the combined effect of both these updates.

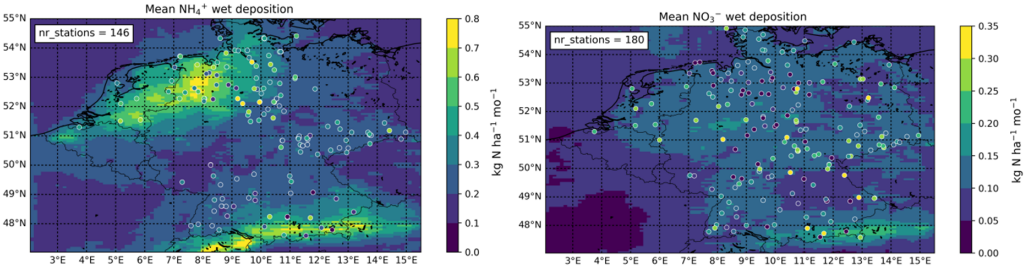

Figure 15: The mean NH_4^+ (left) and NO_3^- (right) wet deposition in kg N ha^{-1} mo^{-1} in 2014.The mean observed wet deposition observed at the stations is plotted on top.

https://doi.org/10.5194/gmd-2019-256
Preprint. Discussion started: 1 October 2019

Geoscientific Model Development Discussions

	Network	Run ID	r	RMSE	Slope	Intercept
NH_4^+ wet deposition	UBA n = 139	$LE_{default}$	0.38	0.30	0.75	0.03
		LE_{z0}	0.38	0.30	0.74	0.03
		LE_{LAI}	0.38	0.31	0.77	0.02
		LE_{z0+LAI}	0.38	0.31	0.76	0.02
	LMRe n = 7	$LE_{default}$	0.67	0.25	0.87	-0.01
		LE_{z0}	0.67	0.25	0.87	-0.01
		LE_{LAI}	0.66	0.26	0.89	-0.03
		LE_{z0+LAI}	0.66	0.25	0.89	-0.03
NO_3^- wet deposition	UBA n = 173	$LE_{default}$	0.41	0.17	0.53	0.01
		LE_{z0}	0.41	0.17	0.53	0.01
		LE_{LAI}	0.40	0.17	0.53	0.00
		LE_{z0+LAI}	0.40	0.17	0.53	0.00
	LMRe n = 7	$LE_{default}$	0.78	0.15	0.60	-0.04
		LE_{z0}	0.78	0.15	0.61	-0.04
		LE_{LAI}	0.78	0.15	0.61	-0.04
		LE_{z0+LAI}	0.78	0.15	0.61	-0.04
NH_3 surface concentration	MAN n = 239	$LE_{default}$	0.60	3.13	1.18	-1.17
		LE_{z0}	0.60	3.15	1.19	-1.17
		LE_{LAI}	0.61	3.34	1.30	-1.62
		LE_{z0+LAI}	0.61	3.35	1.31	-1.62
	EMEP n = 20	$LE_{default}$	0.81	1.38	1.08	-0.03
		LE_{z0}	0.82	1.36	1.10	-0.07
		LE_{LAI}	0.81	1.45	1.15	-0.13
		LE_{z0+LAI}	0.82	1.44	1.16	-0.16
NO_2 surface concentration	Airbase n = 333	$LE_{default}$	0.75	8.83	0.78	-2.22
		LE_{z0}	0.75	8.76	0.79	-2.41
		LE_{LAI}	0.75	9.14	0.74	-1.93
		LE_{z0+LAI}	0.75	9.08	0.76	-2.09

695 **Table 5: Correlation coefficient r, root-mean-square difference, slope and intercept of the different in-situ networks in comparison with the corresponding values from the different model runs.**

https://doi.org/10.5194/gmd-2019-256
Preprint. Discussion started: 1 October 2019

Geoscientific Model Development Discussions

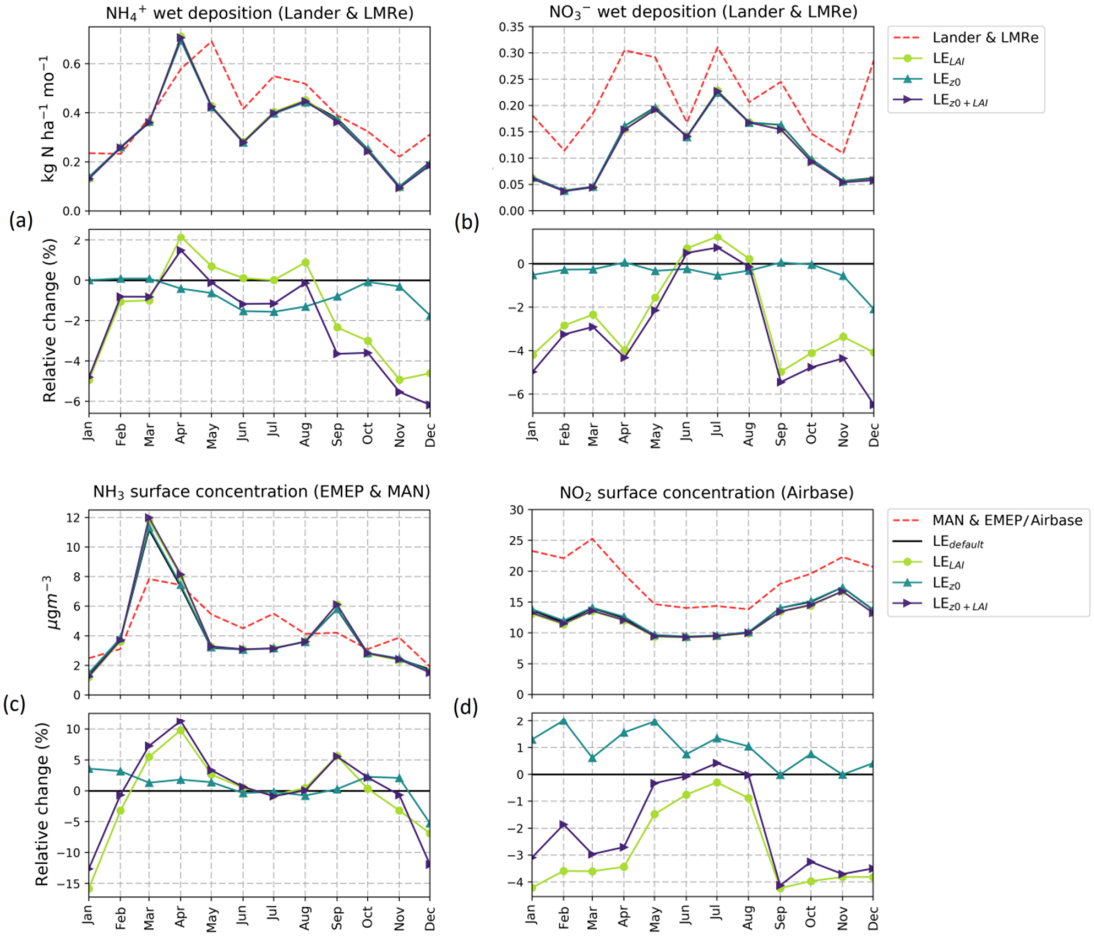

Figure 16: The absolute (top) and the relative (bottom) changes in monthly mean NH_4^+ (a) and NO_3^- (b) wet deposition and NH_3 (c) and NO_2 (d) surface concentrations w.r.t. the default model run induced by the inclusion of the MODIS-LAI and the updated z_0 values. The dotted red line represents the corresponding observations as measured by the in-situ networks.

https://doi.org/10.5194/gmd-2019-256
Preprint. Discussion started: 1 October 2019

Geoscientific Model Development Discussions

Land use categories	Proposed z_0 values (type name)	Reference
Grass	0.008 – 0.03 (short grass, moss)	Wieringa (1993) [1]
	0.02 – 0.06 (long grass, heather)	
	0.03 – 0.6 (categories DEPAC 1)	Silva et al. (2007)
	0.022 (short grassland)	Gallagher et al. (2002)
	0.063 (long grassland)	
	0.01 (mown grass)	Troen and Petersen (1989)
	0.03	Simpson et al. (2012) [2]
	0.1 (grassland)	Bessagnet et al. (2017) [3]
	0.013 (mean DEPAC 1)	This study
Arable land / permanent crops	0.04 – 0.09 (low mature crops)	Wieringa (1993) [1]
	0.12 – 0.18 (high mature crops)	
	0.05 – 0.5 (categories DEPAC 2)	Silva et al. (2007)
	0.1 – 0.5 (categories DEPAC 3)	
	0.12 (arable crop)	Gallagher et al. (2002)
	0.03 - 0.1 (farmland)	Troen and Petersen (1989)
	0.1 – 0.2 (different types of crops)	Simpson et al. (2012) [2]
	0.05 – 0.15 (agriculture)	Bessagnet et al. (2017) [3]
	0.19 (mean DEPAC 2)	This study
	0.20 (mean DEPAC 3)	
Forests	0.8 – 1.6 (mature pine forests)	Wieringa (1993) [1]
	0.6 – 1.2 (categories DEPAC 4 & 5)	Silva et al. (2007)
	1	Troen and Petersen (1989)
	0.8 – 1	Simpson et al. (2012) [2]
	1	Bessagnet et al. (2017) [3]
	2.5	Gallagher et al. (2002)
	1.71 – 1.9 (oak and pine trees)	Lankreijer et al. (1993)
	1.70 – 2.29 (spruce and pine trees)	Yang and Friedl (2003)
	2.91 (mean DEPAC 4)	
	2.55 (mean DEPAC 5)	This study
Urban	0.4 – 0.7 (dense low buildings)	Wieringa (1993) [1]
	0.7 – 1.5 (regularly-built town)	
	0.005 – 1.3 (categories DEPAC 7)	Silva et al. (2007)
	0.5 – 1 (suburbs, city)	Troen and Petersen (1989)
	1	Simpson et al. (2012) [2]
	1	Bessagnet et al. (2017) [3]
	0.92 (mean DEPAC 7)	This study
Other	0.35 - 0.45 (continuous bushland)	Wieringa (1993) [1]
	0.03 – 0.1 (categories DEPAC 8)	Silva et al. (2007) [1]
	0.01 (heathland)	Gallagher et al. (2002)
	0.05 – 0.2 (moorland, scrubs, wetlands)	Simpson et al. (2012) [2]
	0.15 (scrubs)	Bessagnet et al. (2017) [3]
	0.19 (mean DEPAC 8)	This study

Table 6: z_0 values from different types of studies. The first column states the global land use category of the z_0 values. The second column states the (range of) z_0 values, as well as the specific type of land use they are derived for. The third column shows the reference ([1]Literature study, [2]Model input (EMEP MSC-W), [3] Model input (CHIMERE)).

https://doi.org/10.5194/gmd-2019-256
Preprint. Discussion started: 1 October 2019

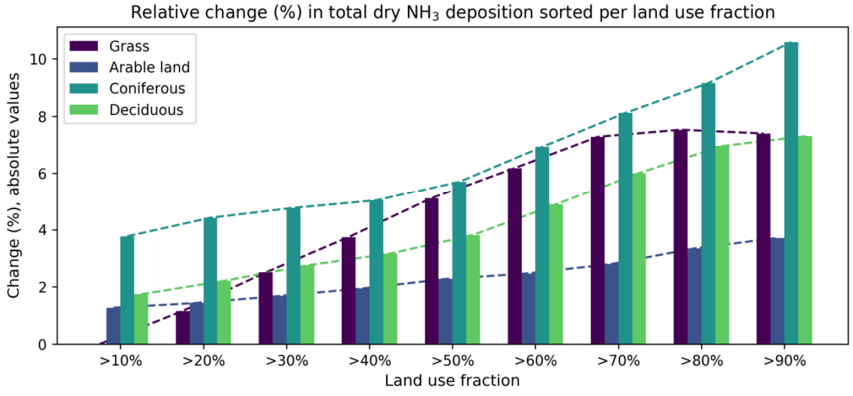

Figure 17: The relative difference (%) in total dry NH_3 deposition in 2014 between the default run ($LE_{default}$) and the run with the updated z_0 values (LE_{z0}), sorted by increasing land use fraction.

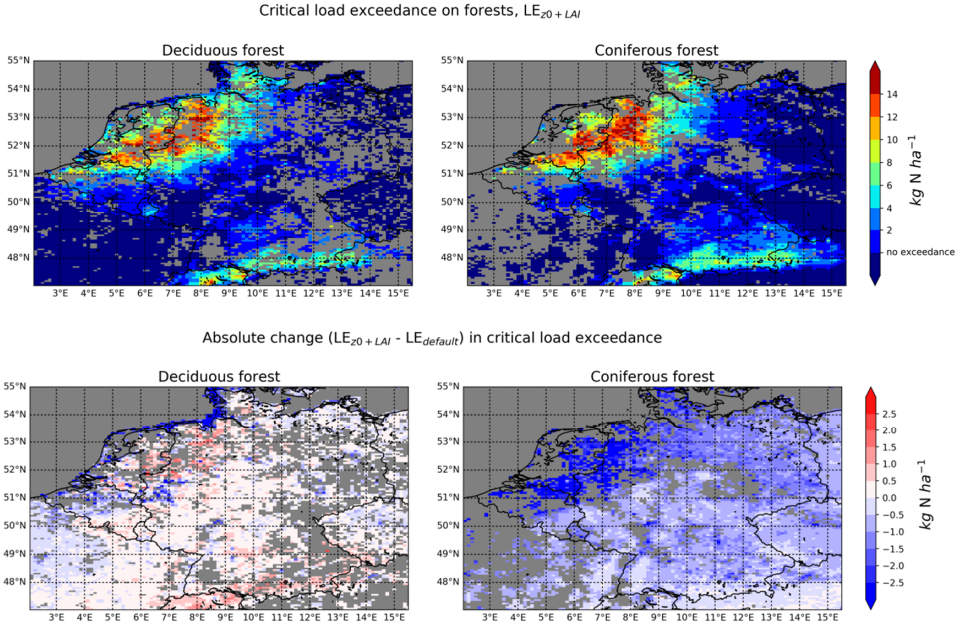

715

Figure 17: Critical load exceedances on forests in kg N ha^{-1} in 2014. The upper figures show the critical on deciduous (left) and coniferous (right) forest, as modelled with the updated z_0 and LAI values. The lower figures show the absolute differences in critical load exceedance on deciduous (left) and coniferous (right) between the new and the default LOTOS-EUROS run.